



Special Feature: Automotive Exhaust Catalyst

Research Report

Numerical Simulation for Optimal Design of a Multifunctional Three-way Catalytic Converter with Detailed Chemistry

Takafumi Yamauchi, Shuichi Kubo, Tomohito Mizukami, Noboru Sato and Norihiko Aono

Report received on Jan. 17, 2011

■ **ABSTRACT** ■ A catalytic reaction model with detailed surface chemistry was developed for a realistic three-way catalytic converter. The reaction mechanisms of this model are based on a set of “quasi-elementary steps” on the active sites of the catalyst surface, and intrinsic kinetic reaction parameters were used for each precious metal (Pt, Rh, and Pd) and cerium oxide (CeO_x). The effect of gas diffusion inside the porous washcoat of the catalyst layer is also considered in order to simulate the precise reactivity of the multifunctional catalyst (multi-layer/zone coating).

Both numerical simulation and experimental studies were conducted for various coating types of the three-way catalysts (Pd/Rh/CeO_2) with an aim to compare the real emissions of multifunctional three-way catalytic converters under a real operating mode (Federal Test Procedure mode).

Comparison of the total mass emissions for each catalyst showed that the NO_x emission of the double layered catalyst ($\text{Rh/CeO}_2/\text{Al}_2\text{O}_3$ layer on $\text{Pd/CeO}_2/\text{Al}_2\text{O}_3$ layer) was lower than that of the single layer catalyst.

We conclude that the double layer coat design has a strong impact on the total mass emissions, especially NO_x emissions, and numerical simulation was effective for catalyst design optimization.

■ **KEYWORDS** ■ Modeling, Catalyst, Simulation, Exhaust, After-treatment

1. Introduction

The demand for lower emission gasoline and diesel engine systems has increased, which necessitates the development of highly effective after-treatment catalysts. The majority of automotive catalytic converters have a monolithic structure, which is coated with an alumina washcoat that supports the noble metal (e.g. Pt, Rh, and Pd) and metal oxides (e.g. cerium oxide, barium oxide). Due to recent advances in catalyst technology, multifunctional catalysts (e.g., layered and zone coated catalysts) are commonly adopted to improve catalyst performance. However, modifications to optimize the catalyst configuration for each engine exhaust system have required time consuming investigations and a large number of experiments.

We have been modeling the catalytic reaction dynamics as one of the most promising approaches to accelerate the effective development of next generation multifunctional catalysts. However detailed reaction mechanisms for the active sites of each catalyst and

the effect of mass transport inside the porous washcoat on the reaction characteristics are not yet fully understood. Therefore, it is very difficult to build a catalytic reaction model that can predict reaction characteristics of a chemical system under a wide range of reaction conditions. In recent years, several proposals have been made for numerical simulations of catalytic converters⁽¹⁻⁴⁾ that have adopted global reaction models to simplify the detailed surface chemistry occurring on the surface. These global reaction models are descriptive only for the range of conditions used for fitting the global rate coefficients, but are not predictive for extrapolated reaction conditions.

An alternate approach is to simulate the chemical reaction by a set of quasi-elementary steps that describe the reactions on a molecular level, the so called microkinetic reaction model. Recently, several researchers have proposed this type of chemical reaction model with detailed surface chemistry.⁽⁵⁻¹⁰⁾ These reaction models have demonstrated the potential to predict the reaction characteristics of catalysts over

a wide range of reaction conditions. In our previous paper⁽⁵⁾ we adopted a microkinetic surface reaction model for an automotive catalyst (a three-way catalyst and a NOx storage-reduction catalyst) to simulate the reaction characteristics of actual after-treatment catalysts, and clarified the effectiveness of the microkinetic reaction model under actual operating conditions.

The purposes of our research are to expand the coverage of the microkinetic reaction model and to simulate the reaction characteristics of the multifunctional three-way catalyst under Federal Test Procedure 75 (FTP75) conditions by utilizing an expanded model. Expansion of our microkinetic reaction model was made as follows: introduction of mass transport both in monolithic channels and the washcoat, and addition of the surface reaction mechanisms on the active sites of Pd and Rh.

2. The microkinetic reaction model

The analytical target in this study is a honeycomb type monolithic reactor. One single channel of the monolith was modeled using a one-dimensional microkinetic reaction model including detailed surface chemistry: adsorption & desorption on the catalyst surface and chemical reactions of adsorbed species on the catalyst active sites.⁽⁵⁻¹⁰⁾

2.1 Outline of the microkinetic reaction model

A detailed multistep reaction mechanism was used to model the surface reactions for a three-way catalytic converter. The surface coverage of the species on the catalyst was also simulated as a function of the position in the single channel of the monolith. The mechanism included only surface chemistry, and gas phase chemistry was neglected, due to the low pressure and temperature, and the short residence time of the species inside the catalyst. The chemistry source terms in the mass conservation equation of gas phase species *i*, due to adsorption/desorption and surface species *i* (adsorbed species) are given by:

$$\dot{s}_i = \sum_{k=1}^{K_s} \nu_{ik} k_{jk} \prod_{j=1}^{N_s} [X_j]^{v'_{jk}} \quad (i=1, \dots, N_s), \dots (1)$$

where *K_s* is the number of elementary surface reactions (including adsorption and desorption), *ν_{ik}* and *v'_{ik}* are the appropriate stoichiometric coefficients, and *N_s* is the number of species adsorbed. The concentration [*X_i*]

of the adsorbed species is given in mol/m³ and equals the surface coverage (Θ_i) multiplied by the surface site density (Γ) and active surface area to volume ratio. The temperature dependence of the rate coefficients is described by a modified Arrhenius expression:

$$k_{jk} = A_k T \exp\left[-\frac{E_{ak}}{RT}\right] \prod_{i=1}^{N_s} \Theta_i^{\mu_{ik}} \exp\left(\frac{\varepsilon_{ik} \Theta_{ik}}{RT}\right) \dots \dots \dots (2)$$

This expression takes additional coverage dependence into account using the parameters μ_{ik} and ε_{ik} . The rate coefficient for adsorption processes is calculated from the initial sticking coefficient *S₀*, which is the sticking probability at vanishing coverage:

$$k_{jk} = S_i^{(0)} \frac{1}{\Gamma^\tau} \sqrt{\frac{RT}{2\pi M_i}}, \dots \dots \dots (3)$$

where τ is the number of occupied adsorption sites of species *i*. and the time variation of the surface coverage Θ_i is given by the following expression:

$$\frac{\partial \Theta_i}{\partial t} = \frac{\dot{s}}{\Gamma} \quad (i=1, \dots, N_s). \dots \dots \dots (4)$$

The equation system was solved using external subroutines to obtain surface coverage and the chemical source term in the gas phase mass and energy conservation equations using the DVODE solver. The active catalytic surface and active surface area to volume ratio were based on literature or experimentally determined values.

2.2 Surface reaction mechanisms

The surface reaction scheme consists of elementary reaction steps on a precious metal and a metallic oxide, e.g., dissociative and non-dissociative adsorption and desorption, and the chemical reactions steps between adsorbed species. Some activation energies are coverage-dependent, due to interactions between the adsorbed species. It was assumed that all species were adsorbed competitively onto each active site. A main part of the surface reaction mechanism has already been authorized in the literature⁽⁸⁾ for numerical modeling of a steady-state three-way catalyst (Pt/Rh Al₂O₃). The kinetic data for the surface reaction mechanisms of CO, H₂, O₂, CO₂, H₂O, C₃H₆ and NO on Pt/Rh active sites were mainly obtained from the literature.⁽⁸⁾ In the previous paper,⁽⁵⁾ the reaction mechanisms for NO oxidation, O₂ storage on cerium oxide, and NO₂ storage on barium oxide were newly

introduced by considering a set of basic experimental results and thermodynamics. It was confirmed that these surface reaction mechanisms successfully predicted the reaction dynamics of the three-way catalyst and nitrogen storage reduction (NSR) catalyst (Pt/Rh/Ce/Ba) in a wide range of reaction conditions. In this paper, we have additionally introduced unknown surface reaction mechanisms of the Pd/CeO₂/Al₂O₃ catalyst and assumed that essential reaction mechanisms on Pd active sites are the same as those on Pt active sites. The surface reaction kinetic parameters were determined by considering the thermodynamics and basic experimental results obtained using the Pd/CeO₂/Al₂O₃ catalyst under various conditions (e.g. catalyst light-off experiment under stoichiometric conditions).

2.3 Modification of the mass transport effect

A two dimensional (2-D) microkinetic reaction model was developed to clarify the mass transport characteristics during the catalyst reaction and to obtain accurate mass transport parameters for construction of a 1-D microkinetic reaction model. A 2-D numerical simulation for the flow field and concentration field in the monolithic reactor was conducted using the lattice Boltzmann method (LBM). The 2-D microkinetic model can directly predict the effects of mass transport by convection and diffusion in both the monolithic channel and the disordered porous Al₂O₃ washcoat layer. **Figure 1** is an example

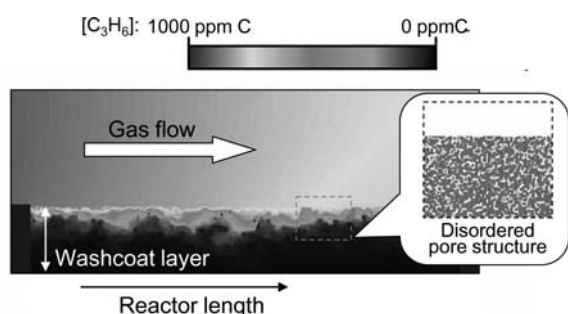


Fig. 1 C₃H₆ concentration contours during C₃H₆ oxidation on Pt/Al₂O₃ @T=300°C (2-D microkinetic model).

Reprinted with permission from SAE paper 2008-01-1540
© 2008 SAE International.

of the 2-D numerical simulation, which shows the total hydrocarbons (THC) concentration contours during C₃H₆ oxidation near the Pt/Al₂O₃ catalyst surface. In the 2-D microkinetic reaction model, the minimum pore size for gas phase diffusion was approximately 0.5 μm and the Knudsen diffusion coefficient was adopted for the diffusion inside the micropores of Al₂O₃ particles. A uniform temperature was assumed for all 2-D calculations. The 2-D microkinetic reaction model successfully predicted the reaction characteristics, considering the microstructural effects of the washcoat layer. In the 2-D numerical simulation, the computational domain was still limited in both time and scale due to the large computational cost, which demonstrates how the 2-D microkinetic reaction model has not yet been able to be applied directly to a full-size catalyst simulation.

2.3.1 Parameter determination of mass transport equations

A 3-layer model was adopted in the 1-D microkinetic reaction model to consider mass transport phenomena inside the monolithic reactor. The 3-layer model consists of one gas phase layer for the channel flow and 2 layers for the porous washcoat. The mass balance equation between each computational domain was solved by considering convection and diffusion.

The mass transport between the gas phase layer and the upper layer of the porous washcoat was described using the film model.⁽¹¹⁾ The Sherwood number Sh_z , as a function of reactor length z in the film model, was determined by utilizing the information from 2-D numerical simulations under various conditions (temperature, flow rate and cell density).

An effective diffusion coefficient of species i , $D_E(i)$, was adopted for the diffusive mass transport between two washcoat layers. The effective diffusion coefficient $D_E(i)$ is described by the following well-know expression.

$$D_E(i) = \frac{\varepsilon}{\tau} D_0(i) \quad \dots \dots \dots (5)$$

where ε is the porosity, τ is the tortuosity of the porous washcoat, and $D_0(i)$ is the bulk diffusion coefficient of species i , respectively. These unknown parameters are dependent on the microstructure of each washcoat material and were determined by both information obtained from 2-D numerical simulations and experimental measurements.

3. Experimental

3.1 Test Catalysts

For this study, several types of three-way model-catalysts were prepared with a basic composition of platinum, rhodium, palladium, cerium oxide and alumina. All catalysts were honeycomb monolith types with a single or double layered washcoat that were degreened under very mild conditions (slightly fuel rich engine operation, 500°C for 5 h).

3.2 Engine dynamometer test

Engine dynamometer experiments were conducted using a 2.4 L gasoline fueled engine. The three following test experiments were conducted for clarification of the reaction dynamics over a wide range of reaction conditions.

1. A/F (ratio of fuel to air in the engine under operation) sweep test: A/F was continuously changed from a fuel rich to a fuel lean condition at a constant inlet gas temperature.
2. Light-off test: the inlet gas temperature was continuously increased at a stoichiometric A/F condition (constant engine operation) using a heat exchanger.
3. A/F rich-lean switching experiment: A/F was periodically changed between fuel rich and fuel lean conditions at a constant inlet gas temperature.

The details of each experimental condition are explained in the following section.

3.3 Vehicle test

A 2.4 L L4 NA gasoline fueled engine vehicle (LEV2/Bin5) was used for the FTP75 test. Catalysts were set in the position of a regular close-coupled converter.

4. Results and discussion

4.1 Validation of the 1-D microkinetic model

4.1.1 Validation of the mass transport model

Two Pt/Al₂O₃ model-catalysts, shown in Fig. 2, were prepared for validation of the 1-D mass transport model; a regular Pt/Al₂O₃ catalyst and a Pt/Al₂O₃ catalyst covered with a dummy Al₂O₃ layer. Validation

of the 1-D mass transport model was performed by comparison of the catalyst reaction characteristics of the Pt/Al₂O₃ model catalysts determined by simulation and experiment. The test conditions used are given in Table 1.

Figure 3 shows the relationship between the simulated emission increase factor (predicted R_E) and the experimental emission increase factor (measured R_E). The emission increase factor (R_E) was defined by

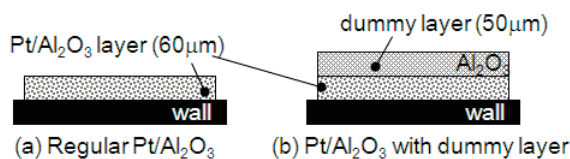


Fig. 2 Schematics of the tested catalysts.

Reprinted with permission from SAE paper 2008-01-1540 © 2008 SAE International.

Table 1 Testing conditions (A/F sweep test).

parameter	value	unit
catalyst volume	0.448	L
cell density	600	cpai
gas flow rate	18.5	g/s
inlet gas temp.	460	°C
A/F range	13.5→15.0	-
A/F sweep rate	0.075	1/min

Reprinted with permission from SAE paper 2008-01-1540 © 2008 SAE International.

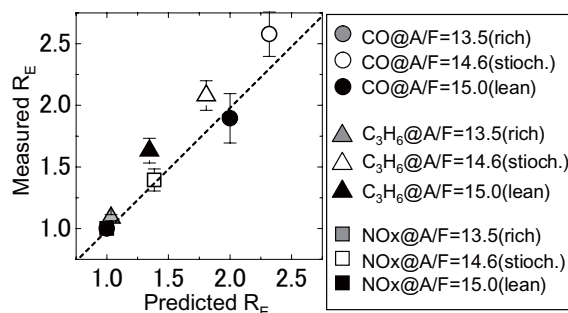


Fig. 3 The effect of the dummy layer (Exp. vs. Model), R_E : The emission increase factor by the dummy layer.

Reprinted with permission from SAE paper 2008-01-1540 © 2008 SAE International.

the following expression:

$$R_E = \frac{[\text{outlet conc.}] \text{ of the catalyst with dummy layer (Fig.2(b))}}{[\text{outlet conc.}] \text{ of the catalyst without dummy layer (Fig.2(a))}} \dots \dots \dots (6)$$

Good agreement was reached between the experimental R_E and that determined by numerical simulation for all conditions (Fig. 3), which confirmed that the 1-D mass transport model can accurately predict the effects of diffusive mass transport inside the washcoat layer.

There was a tendency that R_E became larger under stoichiometric conditions (white colored plots) than under other conditions (fuel rich conditions: gray colored plots, fuel lean conditions: black colored plots). This characteristic indicates that the dummy layer has a strong impact on the emission under stoichiometric conditions, because the overall reaction rate under stoichiometric conditions is limited by gas diffusion in the porous washcoat layer due to the very fast reaction kinetics under stoichiometric conditions.

4. 1. 2 Validation of the surface reaction kinetics on the Pd catalyst

The reaction characteristics of the Pd/CeO₂/Al₂O₃ catalyst were investigated to validate the surface reaction kinetics on the Pd active sites over a wide range of A/F conditions. The test conditions used are listed in **Table 2**.

Figure 4 shows both the experimental and simulated catalyst outlet concentration profiles of THC (including methane) and NOx during A/F sweep operation from A/F = 13.5 to 15.0.

The predicted THC concentration profile is in

excellent agreement with the experimental THC concentration profile (Fig. 4(a)). The present model can express the effects of catalyst deactivation under fuel lean conditions (T = 700-1200 s), which is caused by oxygen adsorption on the Pd active sites (reversible poisoning).

In contrast, Fig. 4(b) shows that the present model fails to predict the reaction characteristics for NOx emissions in the fuel rich region (t = 0-500 s). Although a good agreement was obtained between the experimental result and model prediction for the outlet NOx concentration at t = 0 s, the experimental outlet NOx concentration gradually increased with time, while the predicted outlet NOx concentration decreased with time. In the present microkinetic reaction model, all hydrocarbon species were assumed to be single C₃H₆ components. However, in the engine exhaust gas flow some specific hydrocarbon species must be present that have strong adsorption kinetics to the platinum group metal (PGM) active sites. These hydrocarbons species are supposed to be responsible for the gradual degradation of NOx reactivity, because a very small amount of these hydrocarbons has the

Table 2 Testing conditions (A/F sweep test).

parameter	value	unit
catalyst volume	0.448	L
cell density	600	cpai
gas flow rate	15.5	g/s
inlet gas temp.	460	°C
A/F range	13.5→15.0	-
A/F sweep rate	0.075	1/min

Reprinted with permission from SAE paper 2008-01-1540 © 2008 SAE International.

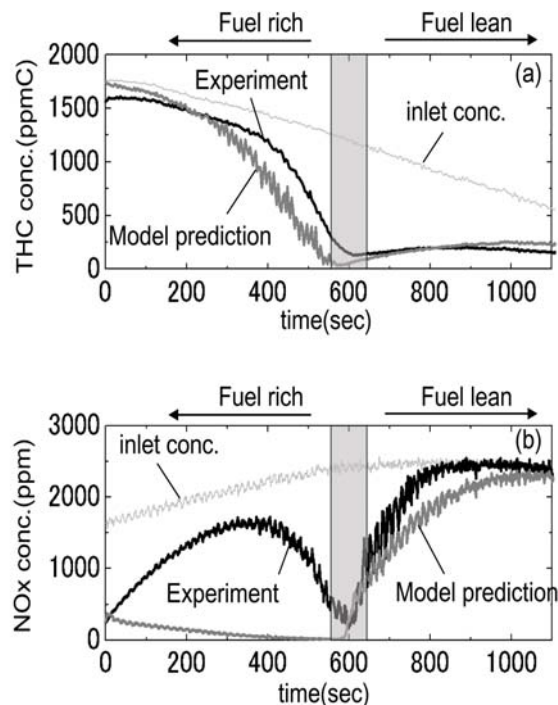


Fig. 4 Outlet concentration profiles during A/F sweep experiments for the Pd/Al₂O₃ catalyst: (a) THC conc. and (b) NOx conc. profiles.

Reprinted with permission from SAE paper 2008-01-1540 © 2008 SAE International.

potential to cause slow catalyst poisoning of the PGM (Pd) active sites. This slow degradation of the NOx reactivity during long fuel rich operation is referred to as a RICH NOx emission. However, the detailed mechanism of the RICH NOx is not yet fully understood, so that the influence of RICH NOx is not successfully covered by the present model. However, under actual engine operating conditions, long term fuel rich operations are not dominant; therefore, the influence of RICH NOx observed for long term fuel rich operation was neglected in this study.

4. 2 Analysis of various multifunctional catalysis

The validation of the 1-D microkinetic model was confirmed for a wide range of reaction conditions, both for the mass transport model inside the porous washcoat and for the detailed surface reaction mechanisms of Pt/Rh/Pd/CeO₂/Al₂O₃. In this section, the reaction dynamics of multifunctional three-way catalysts under the FTP75 test for vehicle emissions regulations are discussed with respect to a numerical simulation.

4. 2. 1 Multifunctional three-way catalyst

Four different multifunctional catalyst configurations were used for this study. Schematics of the catalyst configurations are shown in Fig. 5. Figures 5(a), (b), (c) and (d) show a regular single layered catalyst, a double layered catalyst with Rh/CeO₂/Al₂O₃ in the upper layer, a double layered catalyst with Pd/CeO₂/Al₂O₃ in the upper layer, and a zone-coated catalyst with Pd/CeO₂/Al₂O₃ in the front region, respectively. The common catalyst properties for these catalysts are listed in Table 3. All the catalysts were

degreened under very mild conditions (slightly fuel rich engine operation, 500°C for 5 h) and the total amount of loaded catalyst (Pd, Rh, cerium oxide and alumina) was set to be the same for all the catalyst types.

4. 2. 2 Determination of active PGM sites

In numerical simulation using the microkinetic reaction model, the number of active PGM (Pt/Rh/Pd) sites is the most important unknown parameter. The number of active PGM sites must be determined experimentally, because all loaded PGM atoms do not function as active sites, and the number of active sites is strongly dependent on the catalyst preparation and aging conditions. The PGM effectiveness factor η , is defined by the following expression as a function of the number of active sites.

$$\eta = \frac{\text{the number of the active sites of PGM}}{\text{the total number of the loaded PGM atoms}} \times 100(\%) \quad \dots \dots \dots (7)$$

η should be determined in the kinetic control region, i.e. the reaction characteristics just below the catalyst light-off temperature. Therefore, a light-off test was conducted to determine η for Catalyst-A. The conditions for this experiment are listed in Table 4. The carbon monoxide (CO) light-off temperature, where the conversion of CO reaches 50% ($T_{CO50\%}$), was adopted as a standard value for the estimation of η . $T_{CO50\%}$ for Catalyst-A was experimentally obtained ($T_{CO50\%} = 303^\circ\text{C}$).

Figure 6 shows $T_{CO50\%}$ calculated using the present model with various values of η for Catalyst-A. $T_{CO50\%}$ tends to decrease as η increases. η for Catalyst-A was determined to be 1.3%, according to the experimental $T_{CO50\%}$ value shown in Fig. 6. The values of η for the

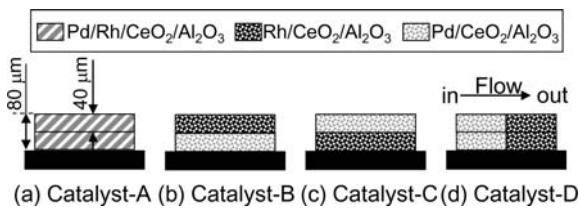


Fig. 5 Schematic of multisegment configurations for multifunctional three-way catalysts.

Reprinted with permission from SAE paper 2008-01-1540 © 2008 SAE International.

Table 3 Catalyst properties.

parameter	value	unit
catalyst diameter	105.7	mm
catalyst length	101.6	mm
catalyst volume	0.892	L
cell density	600	cpai
washcoat thickness	80	μm

Reprinted with permission from SAE paper 2008-01-1540 © 2008 SAE International.

other catalyst types (Catalyst-B-D) were assumed to be exactly the same as that of Catalyst-A ($\eta = 1.3\%$), because the conditions of catalyst preparation or catalyst aging were the same for all catalysts.

The number of active sites for cerium oxide, which function as an oxygen storage capacity, must also be determined experimentally. Detail of the assumptions and a description of the reaction kinetics for cerium oxide have been previously reported.⁽⁵⁾ An A/F rich-lean switching experiment was conducted for Catalyst-A to determine the number of active sites for cerium oxide. The total number of active sites for cerium oxide was also assumed to be the same for all the catalysts (Catalyst-A-D).

4.2.3 Prediction of mass emissions during the FTP75 cycle

The number of active sites for all the catalysts was successfully determined from basic experimental

considerations, as explained in the former section. Therefore, all the kinetic parameters required for the present microkinetic reaction model were already obtained for the multifunctional catalyst simulation. Calculations were performed for the 4 catalysts under a cold transition phase of FTP75 (cycle 1) and the simulated results compared with the experimental results.

Figure 7 shows both the predicted and experimental catalyst bed temperature profiles at the center of the front catalyst region of Catalyst-A during the FTP75 cycle. Catalyst-A became activated around 30 s and there was a significant increase in the catalyst bed temperature caused by heat release of the catalytic reactions. These reaction characteristics can be predicted with good accuracy by the microkinetic model simulation (Fig. 7). The results indicate that the adiabatic temperature condition was realized at the front region of the catalyst in this experimental system. However, there was a slight overestimation in the results for the rear region of the catalyst, according to the model prediction of the catalyst bed temperature. This was mainly due to heat loss to the outer system.

The total mass emission during the cold transition phase of the FTP75 cycle can be numerically obtained by integrating the mass emission rates calculated from the gas flow rate and the reactor outlet concentration. **Figure 8** shows a comparison of the predicted and experimentally obtained total mass emissions for each catalyst type (Catalyst-A-D). Quantitative agreement was successfully achieved between the model prediction and the experimental data for CO and NO_x emissions, although the model prediction tended to slightly underestimate the THC mass emissions. The amount of NO_x emission was the most sensitive to changes in the catalyst multisegment configuration:

Table 4 Light-off testing conditions for Catalyst-A.

parameter	value	unit
gas flow rate	15.5	g/s
inlet A/F	14.5	-
temperature range	200→500	°C
temp. sweep rate	10.0	°C/min

Reprinted with permission from SAE paper 2008-01-1540
© 2008 SAE International.

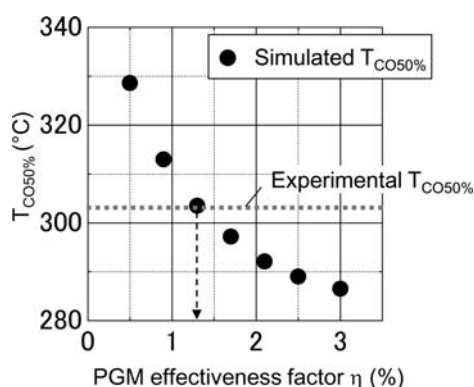


Fig. 6 Light-off temperature $T_{CO50\%}$ simulated for various PGM effectiveness factors η , for Catalyst-A.

Reprinted with permission from SAE paper 2008-01-1540
© 2008 SAE International.

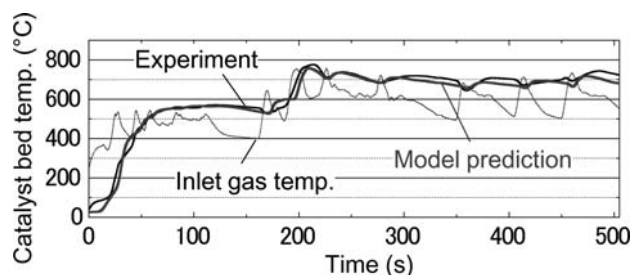


Fig. 7 Time history for the catalyst bed temperature at the center of the catalyst front region for Catalyst-A.

Reprinted with permission from SAE paper 2008-01-1540
© 2008 SAE International.

Catalyst-B had a significant advantage in total NOx emissions compared to Catalyst-A, C, and D. In order to clarify these reaction characteristics for the NOx emissions of the layered catalysts, detailed analyses were performed using the results from the present model calculations.

Figure 9 shows the contribution of NOx emission from both the cold (<300°C: t = 0-40 s) and hot (>300°C: t = 40-505 s) regions to the total NOx emissions for each catalyst type, which was calculated from the predicted results. The main part of the NOx emission originates from the cold NOx emission below 300°C (0-40 s). However, it should be noted that there were significant differences in the amount of NOx emissions, especially in the hot region (40 = -505 s), between each catalyst type (Catalyst-A~D). Therefore, the NOx emission in the hot region was the most sensitive to change in the catalyst multisegment configuration. Focus was then made on the reaction dynamics of NOx emission in the hot region after 180 s (Fig. 7).

Figure 10 shows the reactor outlet NOx

concentrations for each catalyst type after 180 s. Several NOx emission spikes appeared in the same region (at t ≅ 200, 280, 370, 420, 460 s) for all the catalyst types, and the intensity of these NOx emission peaks was strongly dependent on the catalyst multisegment configuration. **Figures 11** and **12** show

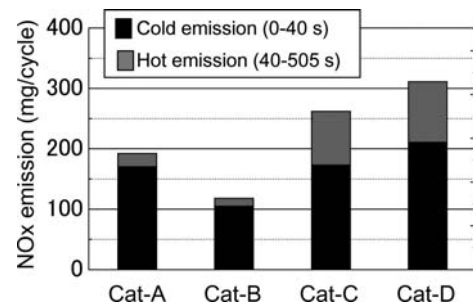


Fig. 9 Predicted NOx emissions from cold and hot regions (cold transition phase of FTP75).

Reprinted with permission from SAE paper 2008-01-1540 © 2008 SAE International.

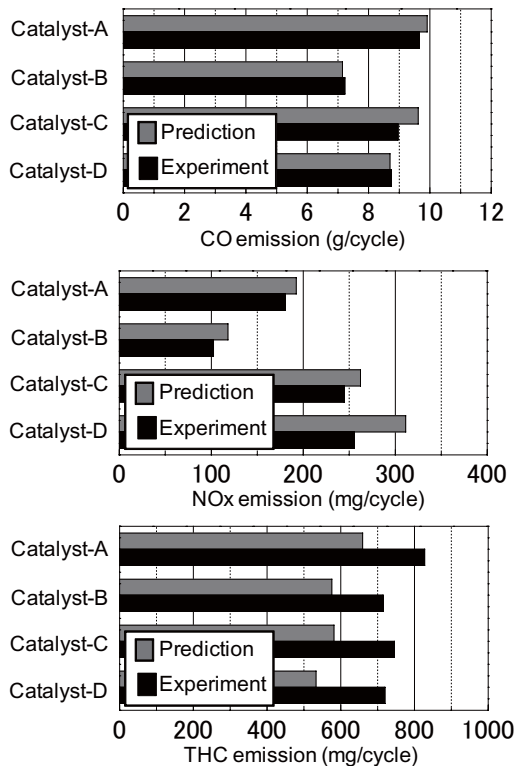


Fig. 8 Total mass emissions for each catalyst type during a cold transition phase of FTP75 (cycle 1).

Reprinted with permission from SAE paper 2008-01-1540 © 2008 SAE International.

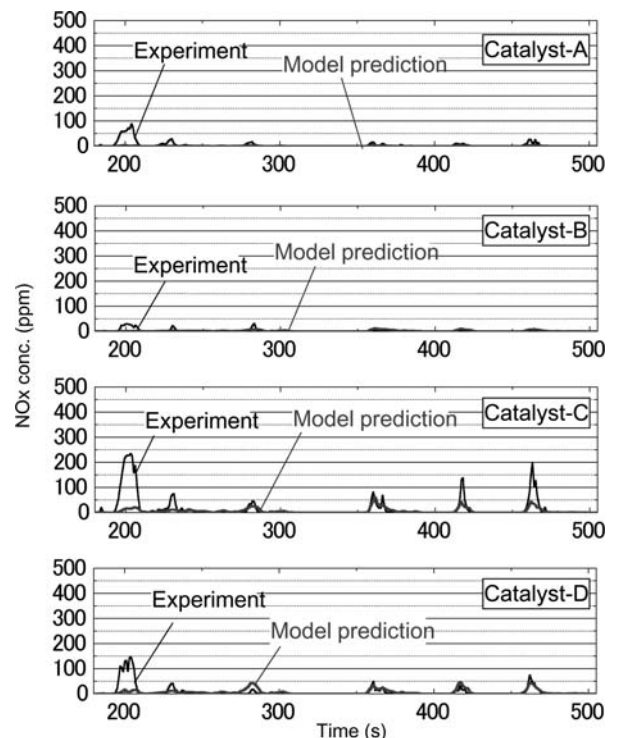


Fig. 10 Outlet NOx concentration profiles in the hot catalyst temperature region for each catalyst type.

Reprinted with permission from SAE paper 2008-01-1540 © 2008 SAE International.

time histories of the inlet gas flow rate and surface coverage of Pd active sites at the center position of Catalyst-A after 180 s, respectively, where CO*-Pd and O*-Pd represent the coverage of carbon monoxide and an oxygen adatoms on the Pd active sites, respectively. Figure 11 indicated several spikes of high gas flow rate that appeared to coincide with the NO_x emission spikes (Fig. 10). When the NO_x emission peaks appeared, the surface coverage of Pd active sites shifted from O*-Pd-rich to stoichiometric or slightly CO*-Pd-rich (Fig. 12). This indicates that the NO_x emissions in the hot region appear under high flow rate and slightly fuel rich conditions. Figure 12 showed no indication of catalyst poisoning by active site occupation during these NO_x emission spikes; therefore, these NO_x emissions are mainly caused by the lack of contact time for NO_x reduction reactions. Comparison with Fig. 10 suggests that the amount of NO_x emission in the hot region is strongly influenced by the catalyst configurations. In other words, the good performance for total NO_x emission over Catalyst-B (see Fig. 9) was achieved mainly due to sufficient suppression of these NO_x emissions by the effective utilization of the active Rh sites in the upper layer.

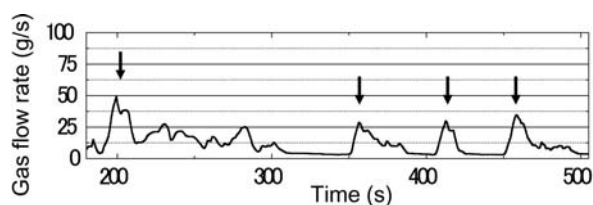


Fig. 11 Time history of inlet gas flow for Catalyst-A.

Reprinted with permission from SAE paper 2008-01-1540
© 2008 SAE International.

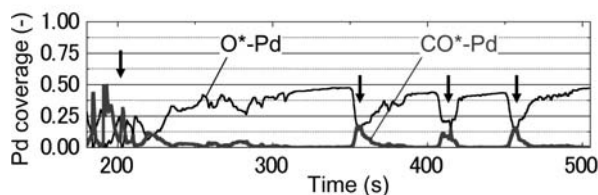


Fig. 12 Time history of Pd surface coverage for Catalyst-A.

Reprinted with permission from SAE paper 2008-01-1540
© 2008 SAE International.

For NO_x emissions in the hot region, there was no obvious border between the lack of contact time for reaction and the RICH NO_x emitted by poisoning of the active sites, which was not introduced in the present model. The model prediction underestimates the large NO_x peak around $t = 200$ s in Fig. 10; therefore, these errors in the model predictions are mainly caused by the influence of the RICH NO_x emissions. The detailed mechanisms for the RICH NO_x emission must be clarified to improve the accuracy of the model prediction by introducing a RICH NO_x model into the present microkinetic reaction model.

From these considerations, it was concluded that numerical simulation using the 1-D microkinetic reaction model could successfully predict both the reaction dynamic characteristics and the total mass emission for various catalyst configurations during the FTP75 cycle with good accuracy, and the characteristics of the catalyst configurations could be extracted.

5. Conclusion

A 1-D microkinetic reaction model considering the mass transport inside the porous washcoat of a multifunctional catalyst was developed in order to clarify the reaction dynamics. Validation of the model was successfully achieved by comparison with a set of basic experiments. It was found that a double layer type catalyst configuration has a significant advantage in total mass emissions, especially NO_x emissions. The reaction mechanisms for these catalysts were numerically clarified with respect to the detailed reaction dynamics as follows. The amount of NO_x emission in the hot catalyst temperature region is sensitive to change in the catalyst multisegment configurations. NO_x emissions in the hot catalyst temperature region are mainly caused by a lack of catalyst contact time for NO_x reduction reactions due to the high flow rate of the exhaust gas.

The present microkinetic reaction model was combined with the mass transport model and could numerically predict the difference in macroscopic catalytic reaction characteristics of various multisegment configurations. Despite the one-dimensionality of the simulation, the model proved to be very effective. The present model can also provide important suggestions for NO_x emission control, which is one of the most important challenges in to

satisfy advanced emission regulations. We have concluded that a numerical simulation approach with detailed surface kinetics should be effective for the further development of high-performance multifunctional catalytic systems.

References

- (1) Koltsakis, G. C., Konstantinidis, P. A. and Stamatelos, A. M., "Development and Application Range of Mathematical Models for 3-way Catalytic Converters," *Appl. Catal. B-Environ.*, Vol.12 (1997), p.161.
- (2) Boehman, A. L., "Numerical Modeling of NO Reduction over Cu-ZSM-5 under Lean Conditions", *SAE Tech. Pap. Ser.*, No.970752 (1997).
- (3) Montreuil, C. N., Williams, S. C. and Adamczyk, A. A., "Modeling Current Generation Catalytic Converters: Laboratory Experiments and Kinetic Parameter Optimization~Steady State Kinetics", *SAE Tech. Pap. Ser.*, No.920096 (1992).
- (4) Jeong, S. J. and Kim, K. S., "A Numerical Approach to Investigate Transient Thermal and Conversion Characteristics of Automotive Catalytic Converter", *SAE Tech. Pap. Ser.*, No.980881 (1998).
- (5) Hickmann, D. A. and Schmidt, L. D., "Steps in CH₄ Oxidation on Pt and Rh Surfaces-high-temperature Reactor Simulations", *AIChE Journal*, Vol.39 (1993), p.1164.
- (6) Deutschmann, O. and Schmidt, L. D., "Modeling the Partial Oxidation of Methane in a Short-contact-time Reactor", *AIChE Journal*, Vol.44 (1998), p.2465.
- (7) Chatterjee, D., Deutschmann, O. and Warnatz, J., "Detailed Surface Reaction Mechanism in a Three-way Catalyst," *Faraday Discuss*, Vol.119 (2001), p.371.
- (8) Dahl, S., Sehested, J., Jacobsen, C. J. H., Tornqvist, E. and Chorkendorff, I., "Surface Science Based Microkinetic Analysis of Ammonia Synthesis over Ruthenium Catalyst", *J. of Catal.*, Vol.192 (2000), p.391.
- (9) Honkala, K., Hellman, A., Remediakis, I. N., Logadottir, A., Carlsson, A., Dahl, S., Christensen, C. H. and Norskov, J. K., "Ammonia Synthesis from First-principles Calculations", *Science*, Vol.307 (2005), p.555.
- (10) Welty, J. R., Wicks, C. E and Wilson, R. E, *Fundamentals of Momentum, Heat, and Mass Transfer*, 3rd ed.; Chapter 26 (1984)
- (11) Olsson, L., Person, H., Fridell, E., Skoglundh, M. and Andersson, B., "A kinetic Study of NO Oxidation and NO_x Storage on Pt/Al₂O₃ and Pt/BaO/Al₂O₃", *J. of Phy. Chem. B*, Vol.105 (2001), p.6895.

Takafumi Yamauchi

Research Field :

- Research & development of the thermal management system

Academic Societies :

- The Japan Society of Mechanical Engineers
- Society of Automotive Engineers of Japan
- Catalysis Society of Japan

Award :

- 56th JSAE Asahara Science Award, 2006



Shuichi Kubo*

Research Field :

- Research & development of the next-generation materials

Academic Societies :

- The Japan Society of Mechanical Engineers
- Society of Automotive Engineers of Japan



Tomohito Mizukami**

Research Field :

- Research & development of Automotive catalyst



Noboru Sato**

Research Field :

- Research & development of Automotive catalyst



Norihiko Aono**

Research Field :

- Research & development of Automotive catalyst



*IBIDEN CO., LTD.
**CATALER CORPORATION